

¹ Chapter 1

² Diamond irradiation study

³ The aim of the study in this chapter is to find the operational limitations of diamond
⁴ detectors for spectroscopy and tracking applications. The chapter contains the mea-
⁵ surement results of data taken with diamond sensors. First the measurement setup
⁶ is described in section 1.1. Then the measured particle spectra are shown in 1.2.
⁷ This is followed by a study of effects of the irradiation damage on the electrical signal
⁸ of the diamond detector. The last section shows the results of the measurements
⁹ of irradiated diamond samples at cryogenic temperatures. The studies compare the
¹⁰ experimentally acquired data with the theory from the previous chapter and define
¹¹ limitations of the diamond detectors in terms of noise, radiation and temperature.

¹² Diamond sensors are mainly used for two types of measurements: particle counting
¹³ and spectroscopy. The first type of measurements depends on the sensor efficiency –
¹⁴ its ability to detect all or at least a known percentage of incident particles. The energy
¹⁵ of the particles is not so important; what bears the information is the rate and the
¹⁶ spatial distribution. Here the particles do not necessarily stop in the bulk, but rather
¹⁷ continue their way. In spectroscopy, on the other hand, the particles stop within the
¹⁸ sensor, depositing all their energy. This energy is then measured by collecting the
¹⁹ freed charge carriers. The goal of the experiments described in this chapter is to:

- ²⁰ 1. Quantify the efficiency of the sCVD diamond in counting mode,
- ²¹ 2. Quantify the degradation of the efficiency as a function of the received radiation
dose,
- ²³ 3. Quantify the macroscopic effects on charge carrier behaviour as a function of
the received radiation dose and
- ²⁵ 4. Define limitations for use in spectroscopy.

²⁶ The results discussed here show that there are several limitations for using diamond as
²⁷ a radiation detector. All of them need to be taken into account when designing a new
²⁸ measurement device. The irradiation study allows for an estimation of the lifetime of
²⁹ the detector and a prediction of the longterm signal degradation as a function of the
³⁰ received radiation dose. The result of the study is a correction factor, which can be

1.1. MEASUREMENT SETUP

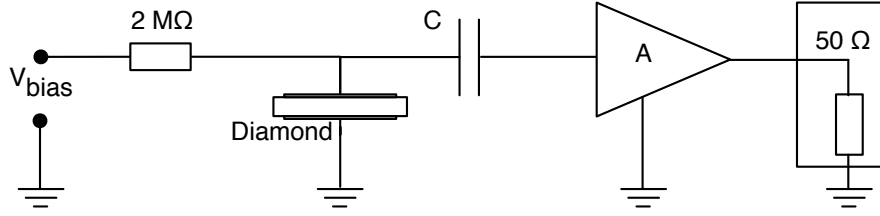


Figure 1.1: Diagram of a diamond detector readout chain.

31 applied during data analysis to ensure that the analysis results are stable despite the
32 detector degradation.

33 1.1 Measurement setup

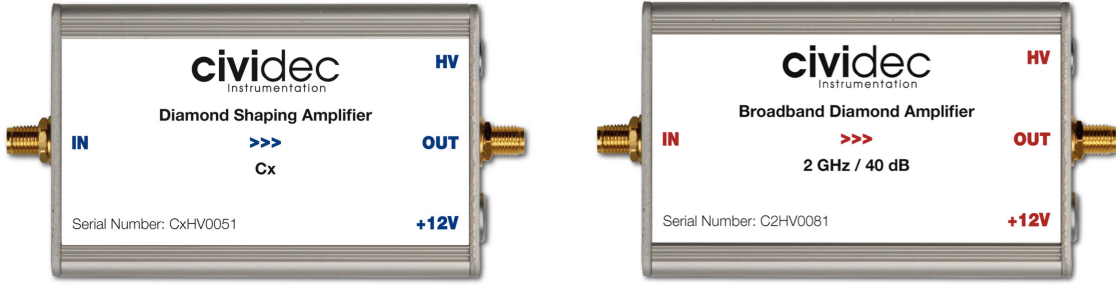
34 The first step of designing a measurement setup is to define the measurement conditions,
35 such as the temperature, the type of radiation and its flux. The second step is
36 to ensure that the setup is insensitive to external electromagnetic interferences and
37 that it minimises electrical noise in the system. The setup needs to be calibrated
38 before use.

39 Shielding has to be applied wherever possible. For instance, aluminium foil can
40 be wrapped around the exposed parts of the system to shield them from external
41 radio-frequency (RF) interferences. In addition, the sensors have to be covered to
42 prevent the exposure to light. The incident photons may deposit enough energy to
43 increase the leakage current of the detector, which produces unwanted results.

44 The measurements using diamond that are explained in these chapters have been
45 carried out using several measurement setups, but they are all similar in terms of
46 the electrical signal chain. The measurement chain consists of three main parts: a
47 diamond sensor, a signal preamplifier and a readout device, as seen in figure 1.1. The
48 signals propagating along the analogue chain are fast – in the GHz bandwidth range –
49 and with low amplitudes – of the order of tens of μV . This gives rise to the importance
50 of RF shielding. Also, the connection between the carrier and the preamplifier has
51 to be as short as possible to avoid capacitive signal losses in the transmission line.
52 Finally, the system needs to be grounded properly.

53 1.1.1 Preamplifiers

54 Two preamplifiers are used for the measurements, one sensitive to charge and the
55 other to current. *CIVIDEC Cx* (figure 1.2a) is a charge sensitive amplifier. Its high
56 SNR is achieved due to a low equivalent noise charge of 300 e^- with an additional
57 30 e^- per each pF of the sensor capacitance. A reported gain of $\sim 12 \text{ mV/fC}$ makes
58 it a good choice for spectroscopic measurements with diamond sensors. *CIVIDEC*
59 *C2* (figure 1.2b) is a fast current preamplifier with a 2 GHz bandwidth limit. It is
60 used for TCT measurements because of its fast response and a good SNR. Both are



(a) Cx charge sensitive preamplifier.

(b) C2 fast charge preamplifier.

Figure 1.2: Amplifiers used for the charge and current measurements.

61 embedded in an RF-tight aluminium box to reduce the noise pickup. Both have an
62 AC coupled input and an output with a $50\ \Omega$ termination.

63 Calibration

64 The amplifiers have to be calibrated before use to determine their gain. Both are
65 calibrated using a square signal generator with a known amplitude step of $U_{\text{in}} =$
66 (252 ± 5) mV. A 2 GHz oscilloscope with a 10 GS/s sampling rate is used to carry
67 out these measurements.

68 **Cx charge sensitive amplifier** calibration necessitates an injection of a well known
69 charge. Therefore the signal from a pulse generator is routed through a capacitor with
70 a calibration capacitance $C_{\text{cal}} = (0.717 \pm 0.014)$ pF and then to the input of the am-
71 plifier. The pulse area behind the capacitor is $a_{\text{cal}} = (5.0 \pm 0.5)$ pVs, with the signal
72 amplitude on the output amounting to $U_{\text{Cx}} = (1.95 \pm 0.05)$ V. The input voltage step
73 combined with the calibration capacitance yields a calibration charge

$$Q_{\text{cal}} = C_{\text{cal}} \cdot U_{\text{in}} = (181 \pm 5) \text{ fC}. \quad (1.1)$$

74 The gain of the Cx amplifier when comparing the integrated input charge to the
75 output amplitude is

$$A_{\text{Cx}}^Q = \frac{U_{\text{Cx}}}{Q_{\text{cal}}} = (9.3 \pm 0.4) \text{ mV/fC} \quad (1.2)$$

76 whereas the factor between the area of the input current pulse and the output am-
77 plitude is

$$A_{\text{Cx}}^a = \frac{U_{\text{Cx}}}{a_{\text{cal}}} = (390 \pm 40) \text{ mV/pVs}. \quad (1.3)$$

78 The area-based amplification factor A_{Cx}^a can be used as an estimate for the integrated
79 charge of a current pulse. However, it has a higher uncertainty ($\sim 10\ %$) than
80 the amplitude-based factor A_{Cx}^Q ($\sim 4\ %$) due to the measurement limitations of the
81 oscilloscope.

1.1. MEASUREMENT SETUP

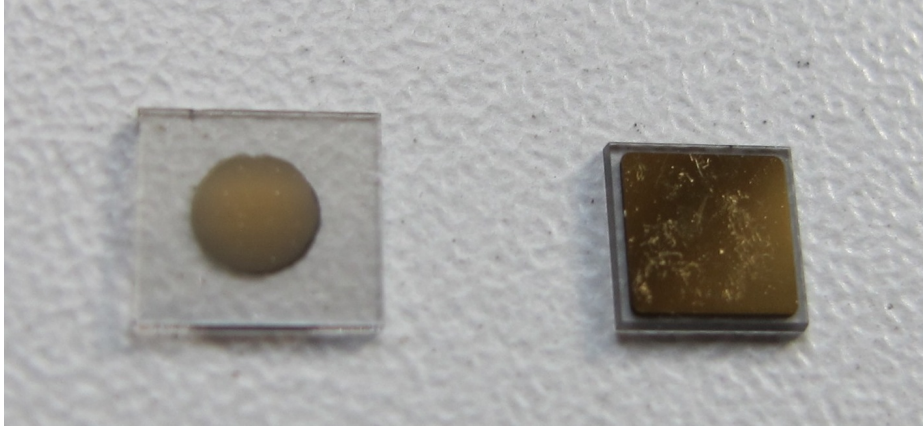


Figure 1.3: Two scCVD diamond samples: A IIa 1scdhq (left) and an E6 S37 (right).

82 **C2 current amplifier** calibration only requires the measurement of the amplitude
83 gain. To keep the output signal amplitude within the ± 1 V linear range of the
84 amplifier, the input signal amplitude has to be minimised. The signal from the
85 generator is therefore routed through a 36 dB attenuator to decrease its amplitude to
86 $U_{\text{inAtt}} = (3.95 \pm 0.05)$ mV. Two amplifiers with different gains have been measured,
87 because both are used for the measurements. The output of the first amplifier amounts
88 to $U_{\text{C2-1}} = (860 \pm 5)$ mV. This yields the amplification gain

$$A_{\text{C2-1}} = \frac{U_{\text{inAtt}}}{U_{\text{C2-1}}} = (217 \pm 3). \quad (1.4)$$

89 The second amplifier has the output equal to $U_{\text{C2-2}} = (632 \pm 5)$ mV with the resulting
90 gain of $A_{\text{C2-2}} = (152 \pm 3)$.

91 1.1.2 Diamond samples

92 Detector-grade diamonds are very difficult to produce. The major challenge is to
93 ensure a high enough purity of the lattice. The sensor samples used for these studies
94 have been acquired from Element Six (E6) [2]. They all have the same standard
95 dimensions. sCVD diamonds with dimensions 4.7×4.7 mm 2 are already sufficiently
96 large for most of the beam monitoring applications and still affordable. One sample
97 with dimensions of 5.6×5.3 mm 2 produced by IIa Singapore [3] has also been char-
98 acterised at CERN [19]. The target thickness for all samples is 500 μm . Diamonds
99 this thick yield a high enough signal-to-noise ratio for MIPs to be measured by the
100 available electronics. Table 1.1 shows all the samples used for this study. Two of
101 them are measured before and after irradiation and then compared. Irradiation doses
102 for damaging the material need to be high – above 10^{12} particles per cm 2 to be able
103 to observe a significant change in behaviour of a diamond sensor.

104	Name	Type	Producer	Dimensions [mm ²]	Thickness [μm]	Electrode	Irradiated
S37	sCVD	E6		4.7 × 4.7	548	Cr/Au	no
S50	sCVD	E6		4.7 × 4.7	537	Cr/Au	no
105	S52	sCVD	E6	4.7 × 4.7	515	DLC/Pt/Au	$3.63 \times 10^{14} \pi \text{ cm}^{-2}$
S79	sCVD	E6		4.7 × 4.7	529	Cr/Au	$1 \times 10^{14} \pi \text{ cm}^{-2}$
ELSC	sCVD	E6		4.7 × 4.7	491	Cr/Au	no
1scdhq	sCVD	IIa		5.6 × 5.3	460	Cr/Au	no

106 Table 1.1: Diamond sensor samples used.

107 The diamond samples have quoted impurity densities of $\leq 2 \times 10^{14} \text{ cm}^{-3}$ and ni-
 108 trogen incorporation of $\leq 10^{-9}$. The electrodes were added by various companies and
 109 institutes. For instance, S52 was metallised by a company DDL (now defunct) while
 110 the Physics Department of the University of Firenze, Italy metallised the S79. There
 111 are also several techniques for producing the electrodes. The DDL contacts consist
 112 of three layers: DLC (diamond-like carbon)/Pt/Au with 4/10/200 nm thicknesses,
 113 respectively. The metallisation for S79, on the other hand, is made up of Cr/Au
 114 with a total thickness of ~ 400 nm. The area coverage also differs from sample to
 115 sample. Diamonds must not be metallised until the very edge as the proximity of
 116 contacts with a high potential may lead to sparking. However, the areas not covered
 117 by the metallisation are less efficient because the fringe fields at the edges are not
 118 as strong as in between the electrodes. This effectively reduces the sensitive area of
 119 the sensors. In the diamonds used here the effective area is anywhere from 9 mm² to
 120 18 mm². The leakage current through the bulk is below 1 nA, but increases for the
 121 irradiated samples. The capacitance is of the order of (2.0 ± 0.3) pF.

122 1.1.3 Readout devices

123 Electrical signals in diamond detectors are in the GHz frequency range. To preserve
 124 the information in the signals, the readout device with a high bandwidth limit must
 125 be used. For instance, a 250 MHz limit is enough for the spectroscopic measurements
 126 with the Cx charge amplifier, but might be insufficient for the current measurements
 127 with the C2 amplifier.

128 Two devices are used take data shown in this chapter. The first choice is a 2 GHz
 129 LeCroy WaveRunner 204MXi-A. This specific model has a sufficiently high bandwidth
 130 limit for the fast current preamplifier signals. It offers a reliable solution for analogue
 131 signal readout of limited amounts of data. However, its slow acquisition speed is a
 132 bottleneck in a test beam experiment. Its initial 100 Hz readout rate decreases to a
 133 mere 20 Hz within 20 minutes, because every single trigger is saved as a separate file
 134 and the Windows operating system is not capable of handling 10000+ files in a single
 135 directory easily. This is why it has been exchanged with a DRS4 [1], an analogue
 136 readout device developed by PSI, Switzerland. This compact device is capable of
 137 recording up to four waveforms at a time at a steady rate of up to 500 Hz. Its
 138 700 MHz bandwidth limitation is sufficient for the signal from the charge amplifier.

1.1. MEASUREMENT SETUP

139 1.1.4 Setup for the efficiency study using β particles

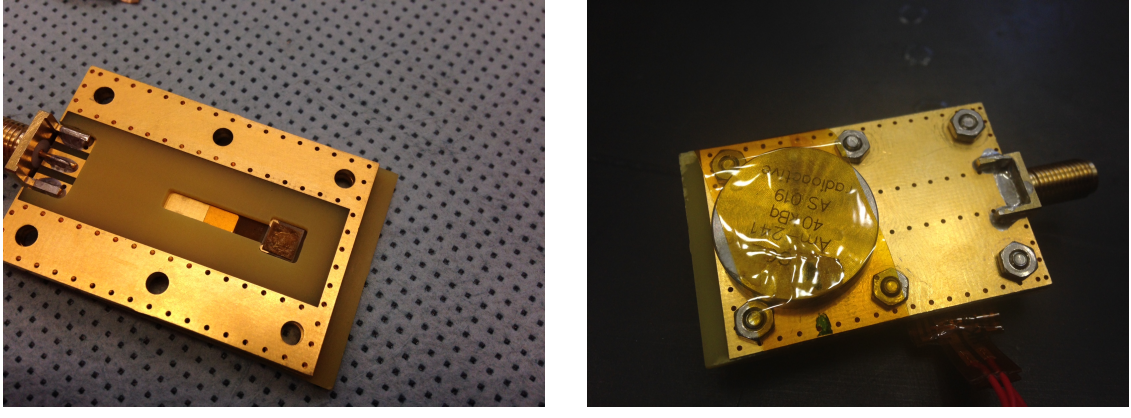
140 The efficiency study of the diamond sensors has been carried out at CERN in the
141 North Hall test beam facility. There a straight high-energy particle beam of 120 GeV π
142 is provided to the users to calibrate their detectors. The beam has a transverse spread
143 of $\sigma = 10$ mm in both axes. The particle rate is of the order of $10^4 \pi \text{ cm}^{-2} \text{ s}^{-1}$. A
144 diamond sensor embedded in a printed circuit board (PCB) carrier has been placed
145 in the beam spot perpendicular to the beam and connected via an SMA connector
146 directly to a charge amplifier. The amplified signal is read out using a LeCroy oscillo-
147 scope and a DRS4 analogue readout system. A computer is used as a controller and
148 data storage for the readout device. A beam telescope is used as a reference detector.
149 It is a device that helps to cross-check the measurements of the devices under test
150 (DUTs) and to carry out spatially resolved studies on the DUTs. It consists of several
151 pixellated sensor planes placed in series, which can track a particle's trajectory with
152 a precision of a few μm . The sensor planes are positioned in front of the DUT and
153 behind it. Then the beam telescope acts as a trigger system – it triggers the readout
154 of both the telescope data and DUT data when both the planes in front and behind
155 the DUT record a hit by an incident particle. A particle detected by all the planes
156 within the DUT window and the DUT itself counts towards its efficiency whereas a
157 hit missed by the DUT means that the DUT is not 100 % efficient. To discard the
158 hits that miss the DUT completely, a region of interest (ROI) can be chosen in the
159 beam telescope planes. The equation for calculating the sensor efficiency is therefore

$$\epsilon = \frac{N_{\text{DUT}} \wedge N_{\text{telescope}}}{N_{\text{telescope}}} \quad (1.5)$$

160 for an ROI smaller than the sensitive region of the diamond.

161 1.1.5 Room temperature α -TCT setup

162 This TCT study is a follow-up of an extensive diamond TCT study at cryogenic
163 temperatures [13]. The room-temperature TCT measurements have been carried
164 out in the laboratory. The setup consists of a diamond sensor embedded in a PCB
165 carrier, a current amplifier and an oscilloscope. To measure α particles, their energy
166 loss during their trajectory has to be minimised. Therefore the diamond is placed
167 inside a vacuum chamber. The chamber is a steel tube with a diameter of 5 cm.
168 On one side it is connected to a vacuum pump via a steel hose. A feedthrough with
169 an SMA connector is placed on the other side. A CIVIDEC C2 current amplifier is
170 connected directly onto the feedthrough. The amplified output is connected to the
171 oscilloscope via an SMA cable. An ^{241}Am source with a diameter of 2 cm and a
172 height of 0.5 cm is fixed onto the sensor carrier (figure 1.4a, figure 1.4b). Then the
173 carrier is inserted in the chamber and fixed in place using an air-tight clamp. The
174 pump can then be switched on. It is capable of providing the inside pressure as low
175 as 10^{-4} mbar after approximately one hour of operation.



(a) PCB carrier with an embedded diamond sample.
 (b) Radioactive source over the carrier.

Figure 1.4: Positioning of the α -source on top of the sensor carrier.

176 1.1.6 Cryogenic α -TCT setup

177 The experiment at cryogenic temperatures has been carried out at the Central Cryo-
178 genic Laboratory at CERN. The room-temperature TCT setup has to be modified to
179 allow for measurements at temperatures as low as 2 K. It consists of three parts:

- 180 1. a cryostat – a thermally insulated cylinder containing liquid helium,
- 181 2. an inlet – an air-tight mechanical tube with valves and feedthroughs at the top
182 that is lowered in the liquid helium and
- 183 3. the diamond sample embedded in a PCB carrier with a fitted temperature
184 sensor, a heater and cables leading to the feedthroughs.

185 The setup is described in detail in [13].

186 When the diamond sample is placed in the PCB carrier and the ^{241}Am source
187 is in place, the inlet is sealed and lowered in the empty cryostat. Then the inside
188 volume of the inlet is evacuated down to 10^{-5} mbar while the liquid helium is flowing
189 into the cryostat. To improve the thermal contact between the diamond and the
190 coolant, a small amount of helium gas is added inside the evacuated inlet, setting
191 the vacuum to around 10^{-3} mbar. This value changes with time, because the gas
192 condenses on the walls of the inlet, reducing the number of floating particles. For this
193 reason the helium gas has to be added on an irregular basis. Every addition causes a
194 significant undershoot of the sample temperature, which has to be corrected for using
195 a heater placed on the back of the PCB carrier. Also, the added gas deteriorates the
196 vacuum inside the inlet. Furthermore, at approximately 60 K the helium gas has to
197 be evacuated from the inlet to avoid a potential explosion due to the expansion of
198 the gas with temperature.

199 When the sample is cooled to the minimum temperature achievable by means of
200 liquid helium without over-pressurising it (4.2 K), the measurements can begin. A

1.2. CHARGED PARTICLE PULSES AND SPECTRA

temperature sensor placed on the back of the PCB carrier is used to measure the temperature of the sample. After every temperature data point, the current through the heater placed in the PCB next to the diamond sample is increased, increasing the sample. The initial temperature time constant of the order of tenths of seconds at low temperatures increases with temperature. Even more so when helium is evacuated from the inlet at 60 K, removing the thermal bridge between the wall of the inlet and the diamond sample. At the room temperature (RT), the time constant is already of the order of minutes.

1.2 Charged particle pulses and spectra

In previous chapter the ionisation profiles for different types of radiation were discussed. β radiation induces a triangular electric pulse whereas α radiation induces a rectangular one. However, their amplitude, width and rise/fall time depend heavily on the type of interaction with the diamond, the purity of the diamond and the bandwidth of the amplifier and the oscilloscope. This section shows the signal pulses of α , β and γ radiation with their respective energy distributions for the case of a diamond detector. This is followed by a discussion of effects of noise on these measurements.

A CIVIDEC C2 current amplifier together with the LeCroy oscilloscope (both with a bandwidth limit of 2 GHz) is used to record the pulse shapes whereas the Cx charge amplifier is used for charge measurements. A 2 GHz bandwidth limit defines the minimum rising time equal to $t_r \simeq \frac{0.34}{BW} = \frac{0.34}{2 \times 10^9} = 170$ ps, therefore the system is capable of measuring pulses with a minimum FWHM $\simeq 170$ ps. This already makes it impossible to measure the initial peak in the α response due to the two opposite charge carriers travelling. If a charge carrier travelling through the bulk takes $t_{t1} \sim 6$ ns to reach the electrode on the opposite side ($d_1 \sim 500$ μm), the carrier with the opposite charge and a shorter path to the closer electrode – max. $d_2 \sim 10$ μm – only takes $t_{t2} \sim \frac{d_2}{d_1} t_{t1} = 120$ ps. A drift time this short induces a current pulse that is too narrow for the C2 amplifier or the oscilloscope to be able to observe.

Figure 1.5 shows a set of pulses and an averaged waveform for α , β and γ radiation using an ^{241}Am , ^{90}Sr and ^{60}Co source, respectively. The particles are measured with the non-irradiated sCVD diamond S37. α particles always produce the same signal pulse, but with a high noise RMS. The averaging suppresses the noise while retaining most the information. It does, however, smear the rising and falling edge, increasing the rising and falling time. The t_r is now of the order of 0.5 ns. Both β and γ pulses look similar - triangular and with a wide range of amplitudes. Here the pulse count is low, so the pulses with a high amplitude are not recorded. A trigger set very high would be needed to “catch” them with the oscilloscope.

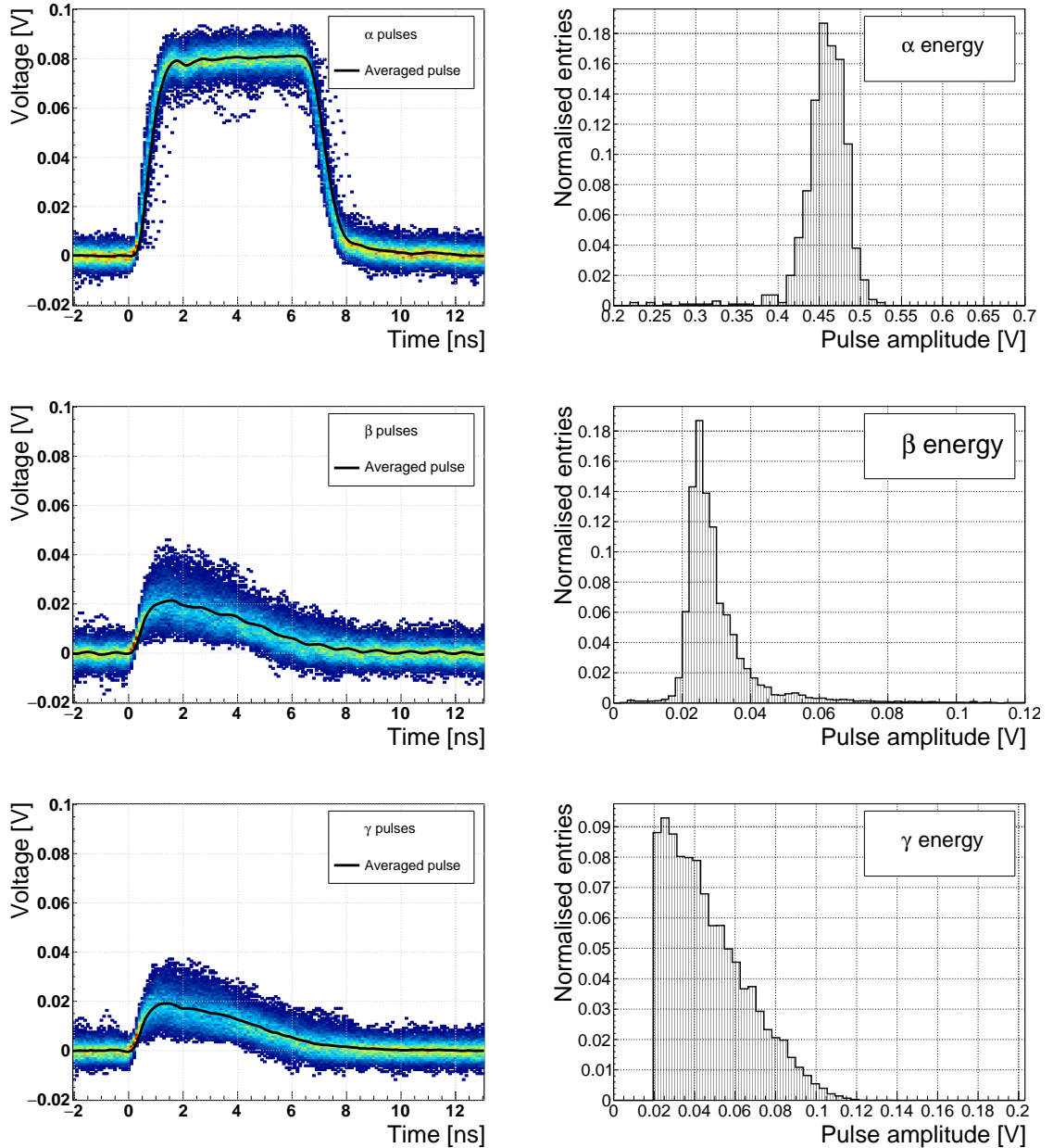


Figure 1.5: Superimposed and averaged pulses (left figures, current amplifier) and distributions of deposited energy (right figures, charge amplifier) for three types of radiation. Note the scale on the X axis of the distributions.

²³⁷ 1.3 Radiation limitations

²³⁸ Exposure to ionising radiation degrades sensors. It deforms the lattice by displacing
²³⁹ the atoms. Various types of lattice defects can be created in diamond, similar to those
²⁴⁰ in silicon: vacancies, interstitials etc. [14] These deformations introduce new discrete
²⁴¹ energy levels between the valence and conduction band. Charge carriers drifting in
²⁴² their vicinity can get trapped, their energy falling to the energy level of the trap.
²⁴³ Their emission back to the conduction band depends on how deep the trap is (how
²⁴⁴ far away from the conduction band it is). The carriers caught in the shallow traps
²⁴⁵ of the order of 100 meV below the conduction band are excited back up already by
²⁴⁶ means of thermal excitation. This phenomenon has a short time constant, dependant
²⁴⁷ on the environmental temperature. Those stopped by deep traps near the middle
²⁴⁸ of the band gap need more energy and thus more time to be emitted to either the
²⁴⁹ conduction or valence band. Some charge carriers remain trapped for long periods. If
²⁵⁰ they build up in a certain region of the diamond and a space-charge forms, it affects
²⁵¹ the surrounding electric field. This is referred to as a space-charge formation. It can
²⁵² either help or counteract the field, depending on the polarity of the trapped carriers.

²⁵³ The energy band jumping goes the other way, too. The carriers in the valence
²⁵⁴ band may use the intermediate energy levels as “stepping stones” to jump to the
²⁵⁵ conduction band and start drifting in the externally applied electric field. These
²⁵⁶ intermediate energy levels are referred to as the generation centres of leakage current.

²⁵⁷ The electrons and holes stopped in these traps cause a decrease of the induced
²⁵⁸ current on the electrodes. This yields a lower integrated charge in an irradiated
²⁵⁹ sensor than that in a non-irradiated one. The charge collection efficiency is therefore
²⁶⁰ correlated with the level of irradiation.

²⁶¹ This section contains a study of the effects of pion ($\pi_{300 \text{ MeV}}$) irradiation on the
²⁶² charge collection efficiency of sCVD diamond detectors. To carry out this study, two
²⁶³ diamond samples were irradiated to doses of $1 \times 10^{14} \pi \text{ cm}^{-2}$ (S79) and to $3.63 \times 10^{14} \pi \text{ cm}^{-2}$
²⁶⁴ (S52). A test beam campaign was carried out to observe the charge collection effi-
²⁶⁵ ciency at different bias voltage settings. The efficiency values acquired are used to
²⁶⁶ determine the effective drop in efficiency as a function of the received radiation dose.
²⁶⁷ This is to test if the collected charge Q is inversely proportional to the received dose
²⁶⁸ Φ . A procedure defined by a collaboration researching diamond behaviour RD42 has
²⁶⁹ been applied to the measured values to extract the damage factor. The next subsec-
²⁷⁰ tion contains measurements and results of a long-term stability study using α and
²⁷¹ β particles. In particular, the charge collection efficiency with β and α radiation as
²⁷² a function of time is measured. To investigate this effect on the scale of charge car-
²⁷³ riers, the change of TCT (transient current technique) pulses with time is observed.
²⁷⁴ Finally, a procedure that improves the pulse shape and with it the charge collection
²⁷⁵ is proposed.

276 1.3.1 Quantifying radiation damage in diamonds

*277 Radiation damage varies with the type of radiation and its energy. There are several
278 models existing [12, 11] that try to explain the impact of irradiation and to provide
279 hardness factors to compare the radiation damage between different particles. The
280 standard way is to convert the damage into 1 MeV neutron equivalent fluence [6].
281 Some models have been extensively verified with simulations and with experiments.
282 In these experiments the charge collection in sensors is measured before and after
283 irradiation. This procedure is repeated several times, with a measurement point
284 taken after every irradiation. Then the charge collection for this set of measurements
285 is plotted as a function of the radiation dose received by a specific particle at a specific
286 energy. From this a damage factor k_λ can be extracted. Damage factors have to be
287 measured across a range of energies and types of radiation to properly quantify the
288 damage in the sensors. Finally they are compared to the simulations to validate the
289 theoretical models.*

*290 Diamond is an expensive material and the technology is relatively new as com-
291 pared to silicon. Therefore few institutes are carrying out diamond irradiation studies.
292 To join the efforts, the RD42 collaboration [5] has been formed. It gathers the exper-
293imental data from diamond irradiation studies. Unlike with silicon, the experimental
294 results so far show no significant correlation with the NIEL (non-ionising energy loss)
295 model [12], which correlates detector efficiency with the number of lattice displace-
296 ments. Therefore an alternative model was proposed [11], correlating the diamond
297 efficiency with the number of displacements per atom (DPA) in the bulk. The idea
298 is that if the recoil energy of an incident particle is higher than the lattice binding
299 energy (42 eV for diamond), the atom is displaced from its original position. The
300 newly formed vacancy acts as a trap for drifting charge carriers. The more displace-
301 ments that form in the bulk, the higher is the probability that a drifting carrier gets
302 trapped. However, different types of particles interact differently with the bulk. In
303 addition the mechanisms of interaction at low energies are different to those at high
304 energies. To assess the damage for individual particles at a range of energies, simu-
305 lations need to be run first. The simulation shown in [11] shows the DPA model for
306 a range of energies of proton, pion and neutron irradiation in diamond. Figure 1.6
307 contains the simulation results as well as the superimposed empirical results of sev-
308 eral irradiation studies. According to the figure, a 300 MeV pion beam damages the
309 diamond bulk twice as much as a 24 GeV proton beam. The data points obtained by
310 RD42 are also added to the figure. They have been normalised to damage by 24 GeV
311 protons. Finally, the data point measured in the scope of this thesis has been added
312 for comparison. The derivation is done below.*

313 Irradiation with a $\pi_{300 \text{ MeV}}$ beam

*314 The samples were irradiated at the Paul Scherrer Institute (PSI) [4] by means of a
315 beam of pions with an energy of 300 MeV (kinetic energy 191.31 MeV) and with a flux
316 of up to $1.5 \times 10^{14} \pi \text{ cm}^{-2}$ per day. The system has a 10 % uncertainty on the beam*

1.3. RADIATION LIMITATIONS

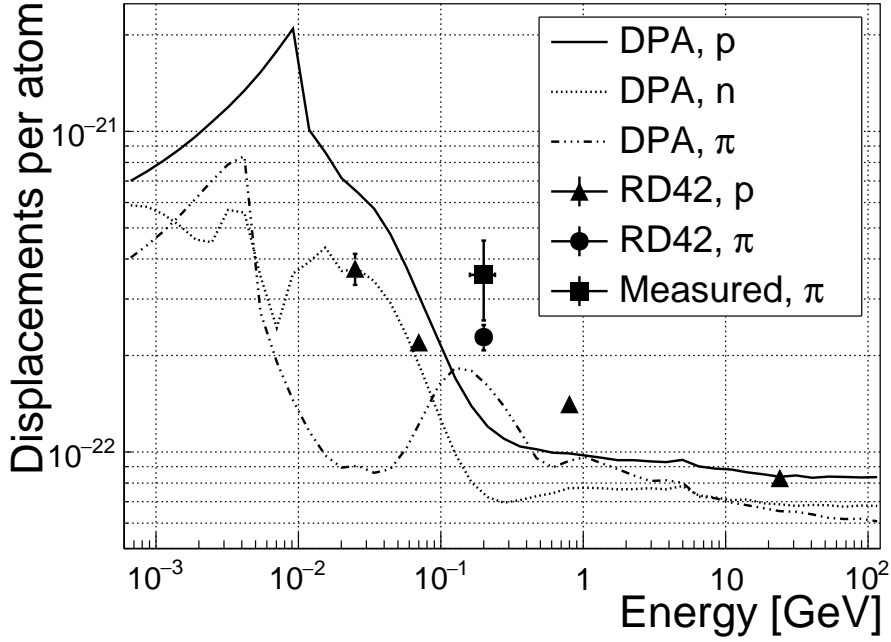


Figure 1.6: Diamond radiation damage - a model based on displacements per atom [11]. The figure shows the DPA as a function of the kinetic energy for protons, neutrons and pions. Added are data points for protons and pions by RD42 [17] and one data point for pions measured in the scope of this study.

energy. Looking at the pion damage curve in figure 1.6, $\pi_{300 \text{ MeV}}$ point (191 MeV kinetic energy) sits on a steep section of the DPA curve. This means that a deviation in beam energy can have a significant effect on the damage in the sensor. In addition, their quoted uncertainty on the measurement of the delivered dose is $\pm 20\%$.

Two diamond samples, S52 and S79, were put in the $\pi_{300 \text{ MeV}}$ beam in the 2014 PSI irradiation campaign; S52 to $(1 \pm 0.21) \times 10^{14} \pi \text{ cm}^{-2}$ and S79 to $(3.63 \pm 0.77) \times 10^{14} \pi \text{ cm}^{-2}$. During the process, the gold electrodes got slightly activated, but the activation decayed in two weeks.

325 Charge collection efficiency and charge collection distance

Three diamonds – non-irradiated S37 and irradiated S52 and S79 – were tested in a $\pi_{120 \text{ GeV}}$ test beam in the SPS North Experimental Area at CERN [8] before and after irradiation. The goal was to estimate the charge collection efficiency (CCE) and charge collection distance (CCD) as a function of irradiation dose. The samples were primed (pumped) prior to data taking using a ${}^{90}\text{Sr}$ radioactive source. The data were then taken at a range of bias voltages ranging from 30 V to 900 V, yielding between 0.06 V/ μm and 1.8 V/ μm electrical field in the bulk. Every data point contained approximately 5×10^4 measured particles. The charge deposited by the particles was measured using a CIVIDEC Cx charge preamplifier.

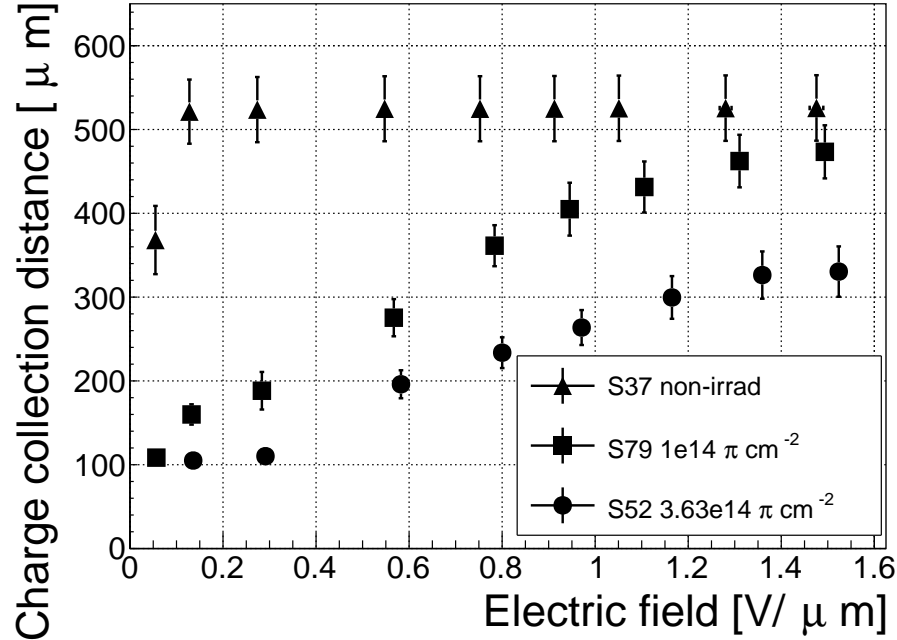


Figure 1.7: The figure shows the CCD for S37, S79 and S52 at a range of bias voltage settings.

As expected, the integrated amplitude spectrum is a Landau distribution. Its most probable value (MPV) is used to calculate the most probable collected charge Q_i :

$$Q_i [e^-] = \frac{1}{1.6 \times 10^{-19}} Q_i [C] = 6241 \cdot Q_i [fC] = 6241 \cdot \frac{MPV [mV]}{A [\frac{mV}{fC}]}, \quad (1.6)$$

where $A = 9.3 \text{ mV/fC}$ is the preamplifier gain factor and $1 e^- = 1.6 \times 10^{-19} \text{ C}$. The CCD can then be calculated using the average number of electron-hole pairs produced per micrometer in diamond $\delta_d = 36 \text{ e-h } \mu\text{m}^{-1}$ (from table ??):

$$CCD = \frac{Q_i}{\delta_d}. \quad (1.7)$$

The resulting CCD for the three measured samples at a bias voltages ranging from $0.2\text{--}1.6 \text{ V } \mu\text{m}^{-1}$ is shown in figure 1.7. S37 exhibits a full collection distance already at $0.4 \text{ V } \mu\text{m}^{-1}$ whereas the irradiated samples have a more gentle increase of CCD with increasing bias voltage. It is evident that at $1 \text{ V } \mu\text{m}^{-1}$ the maximum CCD has not been reached in the case of S79 and S52. Nevertheless, to compare the measured data point with those provided by RD42, the CCD at $1 \mu\text{m}$ has to be taken.

Irradiation damage factor

The irradiation damage factor k_λ is a way to quantify irradiation damage of a specific particle at a specific energy. Via this factor different types of irradiation can be

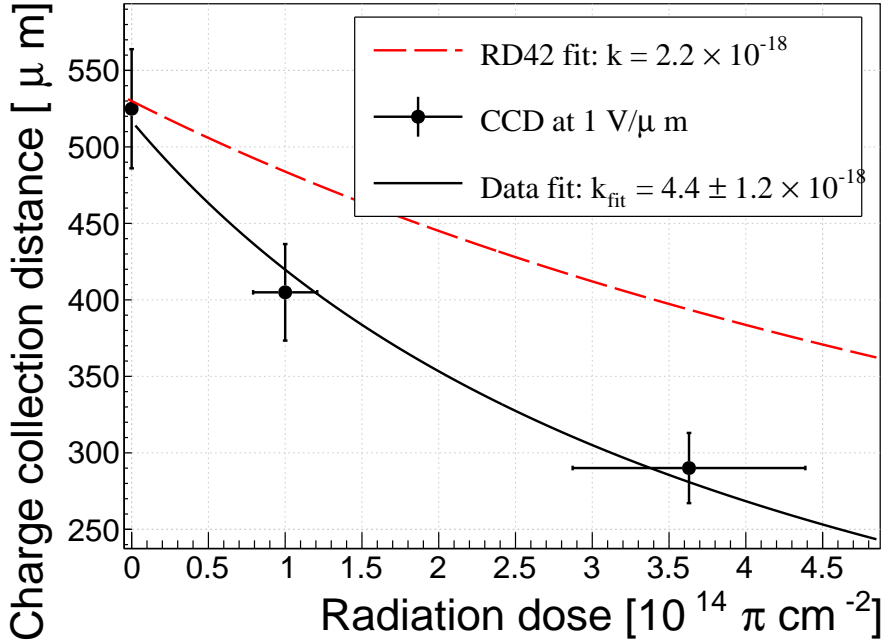


Figure 1.8: The charge collection distance at 1 V/ μm bias voltage for the three diamond samples is plotted as a function of the received radiation dose. It is compared to the RD42 data for pion irradiation. The data points are about 15–25 % lower than expected from the RD42 data [17].

350 compared. It is obtained experimentally by measuring the CCD of a number of
 351 samples at various irradiation steps and fitting the equation 1.9 to the data. λ is the
 352 measured CCD, λ_0 is the CCD of a non-irradiated sample and Φ the radiation dose.
 353 As a reference, the damage factor for 24 GeV protons is set to $1 \times 10^{-18} \mu\text{m}^{-1} \text{ cm}^{-2}$.

$$\frac{1}{\lambda} = \frac{1}{\lambda_0} + k_\lambda \cdot \Phi \quad (1.8)$$

$$\lambda = \frac{\lambda_0}{k_\lambda \lambda_0 \Phi + 1} \quad (1.9)$$

354 The data points with the maximum CCD obtained in the test beam measurements
 355 are plotted against radiation dose received in figure 1.8. Equation 1.9 is fitted to
 356 the data points and a damage factor $k_\lambda = (4.4 \pm 1.2) \times 10^{-18} \mu\text{m}^{-1} \text{ cm}^{-2}$ can be
 357 obtained. The value is for a factor of two higher than the damage factor obtained by
 358 RD42. This could be due to an insufficient priming time ahead of the measurement.
 359 In addition, the diamond samples have not been polished and re-metallised after
 360 irradiation, as is the case for the RD42. Also, with only two samples measured, the
 361 statistical uncertainty is high. Nevertheless, it can be concluded that the 300 MeV
 362 pions damage the diamond bulk significantly more than the 24 GeV protons.

364 1.3.2 Long-term measurement stability

365 An important requirement for particle detectors is a stable performance over long
366 periods of time. For instance, the charge collection for a defined radiation type and
367 quantity must not change over time or has to change in a predicted way. The stability
368 of diamond detectors depends on many factors: material purity, polishing process,
369 electrode material, irradiation damage etc. The aim is to study the behaviour of
370 diamond under controlled conditions, with the goal to understand its limitations.
371 One of these limitations is the received radiation dose as it can affect the long-term
372 stability of the sensor during operation.

373 The three diamond samples (S37, S79 and S52) have been exposed to two different
374 types of ionising radiation for a longer period to see if their behaviour changes over
375 time. Two parameters have been observed in particular:

- 376** 1. Charge collection of β particles and
377 2. Charge collection and ionisation profile of α particles.

378 **β long-term stability**

379 The diamond samples have undergone a long-term stability test at room temperature
380 using β radiation. This has been done using a ^{90}Sr source emitting ~ 2 MeV electrons
381 at a rate of approximately $10^4 \text{ e}^- \text{ cm}^{-2}$. To simulate the initial conditions in HEP
382 experiments, the sensors must not be primed before starting the measurements. The
383 measurement setup consists of a diamond sample (S37, S52 or S79) with the CIVIDEC
384 Cx spectroscopic amplifier, a silicon diode with a CIVIDEC C6 amplifier for triggering
385 and a ^{90}Sr source on top. A particle emitted by the source traverses the sensor bulk
386 and hits the silicon diode, triggering the analogue signal readout. The source is
387 left on the top for the course of the experiment. The measurements, however, are
388 taken at discrete times. For every data point, approximately 10^4 triggers have to be
389 recorded. The offline analysis of the recorded signal pulse amplitudes yields a Landau
390 distribution for every data point. The current charge collection relative to the initial
391 charge collection for every sample is plotted as a function of the received β dose in
392 figure 1.9. It shows that, for the irradiated samples, the charge collection efficiency
393 improves when the diamond sensor is primed with a β source. The effect is negligible
394 for the non-irradiated high-quality S37. Both relative increases are significant – 22 %
395 for S79 and 55 % for S52. At a received dose of approximately 4×10^6 particles the
396 charge collection is stabilised. At that point S79 achieves close to a full efficiency (in
397 absolute values – not shown) whereas S52 reaches approximately 50 %.

398 The ~ 2.28 MeV electrons emitted by this source are not MIPs; their charge depo-
399 sition is higher than that of an electron MIP, according to the Bethe-Bloch distribu-
400 tion [7]. Nevertheless, for the purpose of these measurements this energy is adequate
401 since only the relative change in charge collection is of interest.

402 To sum up, diamond provides a stable measurement of the β radiation detection
403 after reaching a stable state. Even if damaged by radiation, it reaches a stable charge

1.3. RADIATION LIMITATIONS

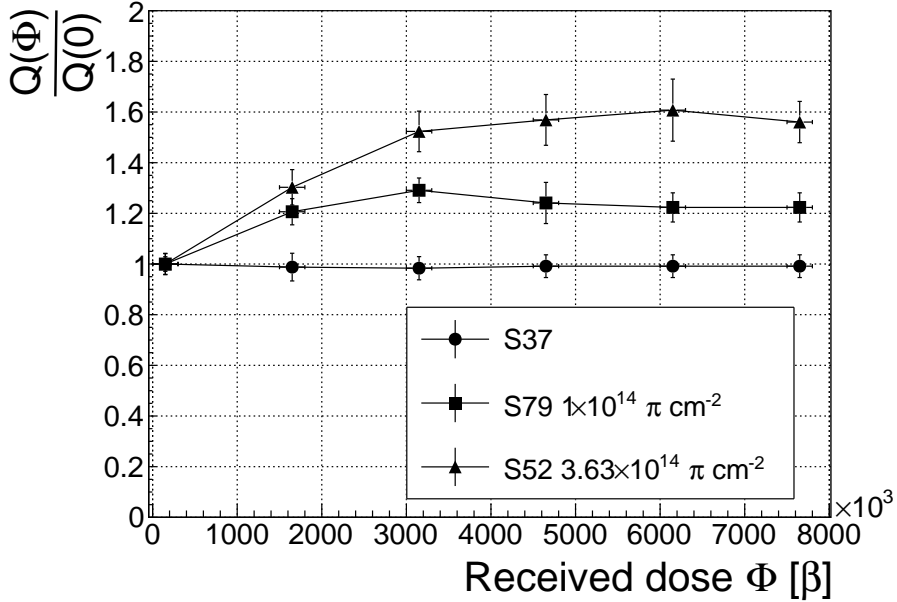


Figure 1.9: Relative increase of charge collection over time due to priming with the ^{90}Sr radioactive source. The charge collection for the non-irradiated S37 stays constant. The bias voltage for this measurement is 1 V/ μm .

404 collection at a received dose of $\sim 4 \times 10^6$ MIPs. Its efficiency decreases with a high
 405 irradiation dose. However, the decrease can be accounted for if the damage factor
 406 and the rate and energy of the particles are known. γ radiation has a similar impact
 407 on the diamond as the β . The incident photons, if they interact with the diamond,
 408 prime the bulk, increasing the charge collection efficiency. The difference, however,
 409 is that the interaction probability (cross-section) is lower for gammas [18, 10].

410 α long-term stability

411 This part discusses the stability of irradiated diamond sensors during α measurements.
 412 An ^{241}Am source has been used, emitting α particles with a mean energy of 5.5 MeV.
 413 They affect the diamond differently than when subjected to β radiation. This is due
 414 to the point-like charge carrier creation; an α particle penetrates the bulk and stops
 415 at a depth of $\sim 14 \mu\text{m}$ (for a 5.5 MeV particle). The deposited energy on its path
 416 produces 4×10^5 e-h pairs according to equation 1.10:

$$n_{\text{e-h}} = \frac{E}{E_{\text{e-h}}} \quad (1.10)$$

417 where E is the deposited energy of the particle and $E_{\text{e-h}}$ is the energy required to
 418 create an electron-hole pair. The deposited energy and as a consequence the collected
 419 charge for a MIP is significantly lower in comparison. According to equation 1.11 a
 420 MIP produces 18×10^3 e-h pairs in a 500 μm thick diamond:

$$n_{\text{e-h}} = d \cdot E_{\text{avg}}, \quad (1.11)$$

421 where d is the thickness of the sensor and E_{avg} is the average number of e-h pairs
422 created per micrometer. Thus the collected charge of a 5.5 MeV α is for a factor
423 of 22 higher. In addition, the energy is deposited in a small volume – 14 μm in
424 depth and \sim 20 nm radially [13]. This dense distribution of charge carriers affects
425 their behaviour at the start of the drift. Furthermore, carriers of only one polarity
426 drift through the sensor while those of the opposite polarity almost instantly reach
427 the adjacent electrode. Taking into consideration that the diamond bulk has been
428 damaged by irradiation, these phenomena combined might have an effect on the
429 operation of the detector.

430 To test the stability of the diamond during α measurements, the samples have
431 been biased at +500 V and exposed to up to 8000 α hits while measuring their charge
432 collection efficiency using the CIVIDEC Cx spectroscopic amplifier. The charge col-
433 lected at every measurement point $Q(\Phi)$ is compared to collected charge of the first
434 measurement $Q(0)$. The resulting ratio $\frac{Q(\Phi)}{Q(0)}$ for all samples is shown in figure 1.10.
435 Each measurement point is an average of 30 consecutive α hits. The conclusions
436 drawn are the following:

- 437 - $Q(\Phi)$ for the non-irradiated S37 is stable as compared to $Q(0)$ over the course
438 of the measurement.
- 439 - The initial efficiency of the irradiated S52 and S79 starts decreasing already at
440 a low α count.
- 441 - The charge collection efficiency of the unprimed irradiated samples drops much
442 faster than after priming.
- 443 - The particle count rate decreases with decreased efficiency, which is clearly seen
444 in the unprimed S52 data where the data points at a low efficiency are much
445 further apart.

446 The absolute values are not shown here because only the relative drop is of interest
447 in the scope of the long-term stability tests.

448 To investigate this sudden drop in efficiency, the current pulse shapes using a
449 CIVIDEC C2 current amplifier have to be observed, as shown in figure 1.11. The
450 shape of the pulse holds more information about the charge carrier properties in the
451 sensor than solely the value of the integrated charge. This time only the primed
452 S79 sample has been tested. Both the hole and the electron collection are observed
453 to determine whether they behave differently or not. The raw acquired data in fig-
454 ures 1.11 show that the initially stable pulses start deteriorating; suddenly several
455 different shapes start appearing, some still very similar to those from the beginning
456 while the others with almost zero amplitude.

457 A more dedicated analysis of the first observation has been carried out as follows:
458 at the beginning of the test when the diamond is still operating stably, 60 pulses are
459 recorded. An average pulse is calculated. This is a reference pulse for the subsequent
460 measurement points. Then an RMS of the individual pulses σ_n with respect to the

1.3. RADIATION LIMITATIONS

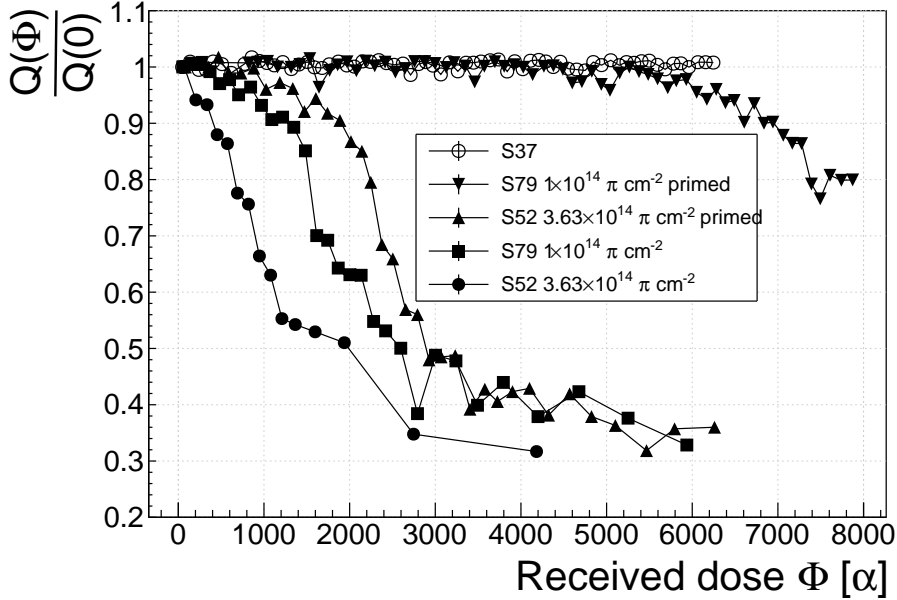


Figure 1.10: A relative drop in charge collection efficiency as a function of the received α dose for non-irradiated and irradiated diamond samples.

⁴⁶¹ reference pulse is calculated and the resulting RMS values are summed together into
⁴⁶² σ_{ref} :

$$\sigma_{\text{ref}} = \sum_{n=1}^{60} \sigma_n. \quad (1.12)$$

⁴⁶³ All the subsequent data points also consist of a set of 60 pulses. At every data
⁴⁶⁴ point the summation of the RMS values of the individual pulses with respect to the
⁴⁶⁵ initial averaged pulse σ is calculated according to equation 1.12. The ratio between the
⁴⁶⁶ initial σ_{ref} and discrete values σ gives a measure of the change of the pulse shape with
⁴⁶⁷ respect to the reference pulse at the start of the measurement. Therefore the initial
⁴⁶⁸ value is 1 and it decreases if the RMS values of subsequent data points are higher.
⁴⁶⁹ Figure 1.12 shows the ratio $\frac{\sigma_{\text{ref}}}{\sigma(\alpha \text{ dose})}$. From the data obtained it can be concluded that
⁴⁷⁰ the initial pulse shape quickly starts deteriorating. In fact, the deterioration of the
⁴⁷¹ shape follows an approximate exponential decay function, which can be fitted to the
⁴⁷² data. The resulting decay constants for electrons and holes are $\tau_e = (4400 \pm 150) \alpha^{-1}$
⁴⁷³ and $\tau_h = (3300 \pm 140) \alpha^{-1}$. The electrons retain the initial shape for longer. The
⁴⁷⁴ deteriorated shapes also seem to be for a factor of 2 better than those of the holes.

⁴⁷⁵ **Discussion** One hypothesis is that this behaviour is caused by space-charge. Some
⁴⁷⁶ moving charges get stopped in the charge traps in the bulk for a long time, building up
⁴⁷⁷ regions of space-charge. The built up space-charge affects the electric field, making
⁴⁷⁸ it non-uniform. The non-uniform field in turn affects the drifting charge carriers,
⁴⁷⁹ slowing them down or speeding them up, depending on the field gradient. Since the

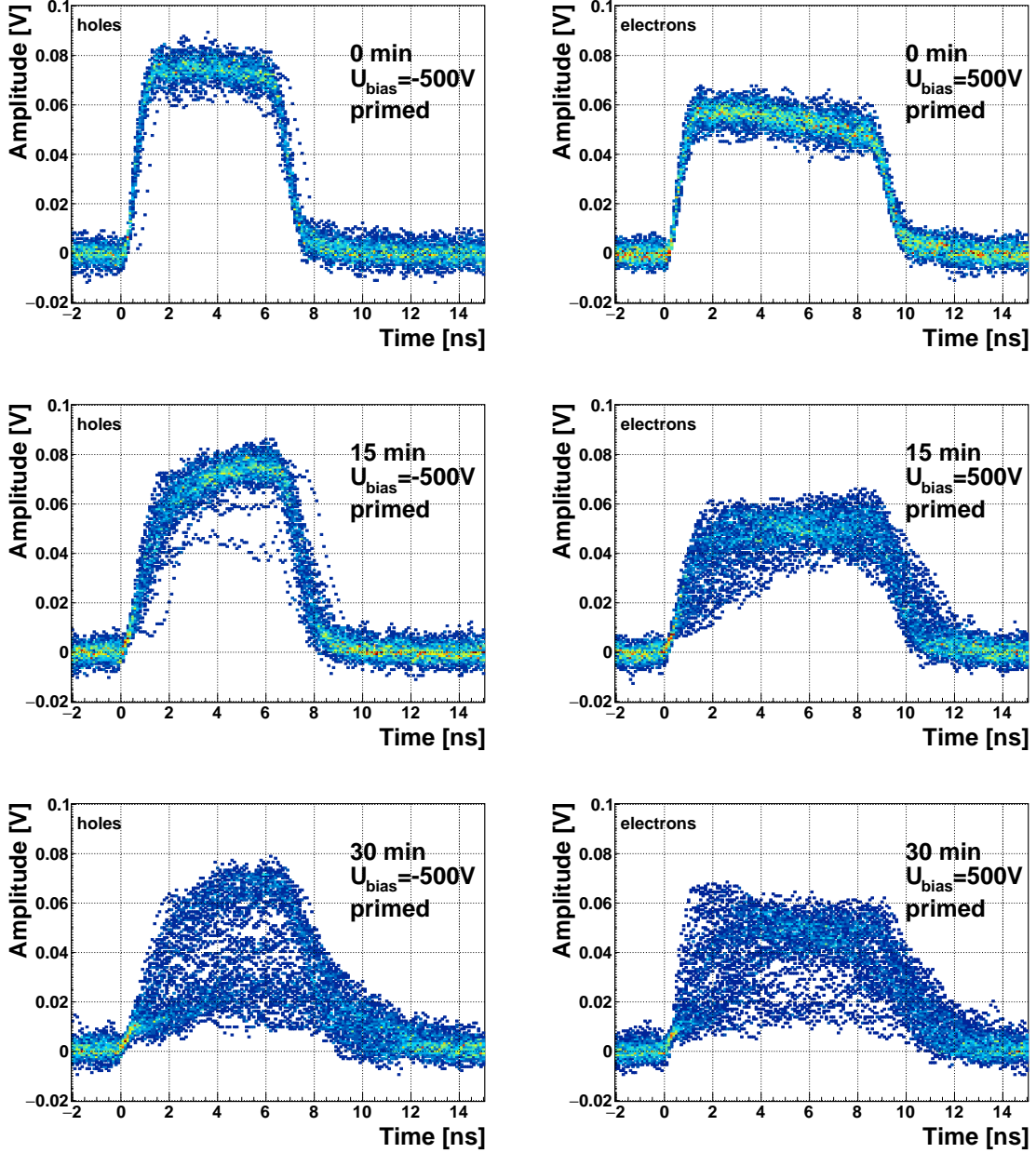


Figure 1.11: The signal of the irradiated and primed S79 deteriorates with time for both polarities. Every plot contains 60 superimposed pulses.

480 movement of the carriers is inducing the electric current, the field gradient can be
481 observed in the current signal.

482 **Restoring the pulse shapes** Finally, an effort has been made to find a way for the
483 pulse shapes to return to their initial state. Five methods are listed:

- 484 1. Removing the source and leaving the bias voltage switched on,
485 2. Removing the source and switching the bias voltage off,

1.3. RADIATION LIMITATIONS

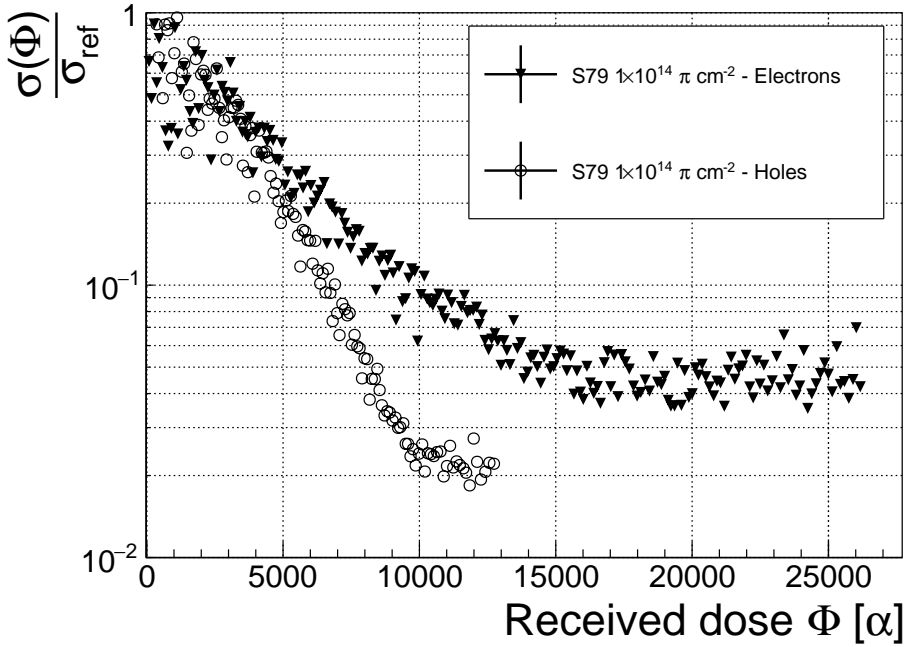


Figure 1.12: Deterioration of the pulse shapes with time.

- 486 3. Priming with γ at a rate of $400 \text{ s}^{-1}\text{cm}^{-1}$ without applied bias voltage,
 487 4. Priming with β at a rate of $1000 \text{ s}^{-1}\text{cm}^{-1}$ with applied bias voltage and
 488 5. Priming with β at a rate of $1000 \text{ s}^{-1}\text{cm}^{-1}$ without applied bias voltage.
- 489 Before starting each method, the diamond sample S79 is first primed using a ^{90}Sr
 490 source for approximately one hour. Then the bias voltage is switched on and an
 491 ^{241}Am source is put on top. The pulses produced by the incident α particles have a
 492 proper rectangular pulse at the beginning, but then start changing – first gradually
 493 and later increasingly more in an erratic way, as described in the text above. After
 494 approximately 30 minutes, one of the methods is tested. When a “healing” procedure
 495 is started, a set of 60 pulses is taken at irregular points of time to observe the change
 496 in the pulse shape and to assess the quality of the “healing” procedure. Then the
 497 bias voltage is switched off and the sample is primed again to reset its state before
 498 starting with the next run.
- 499 The results depicted in figure 1.13 show that the methods (3) and (5) improve the
 500 shape, method (2) helps slowly, (1) does not show any change with time and (4) at first
 501 improves, but then significantly degrades the shape. The effect observed in method
 502 (4) has already been described in [15]. The “healing” process therefore depends on
 503 the rate of radiation, the bias voltage and the time of exposure. The ionising radiation
 504 creates free charges, which quickly recombine close to the place of generation. It is
 505 likely that they also release the charges trapped during the measurement, reducing the

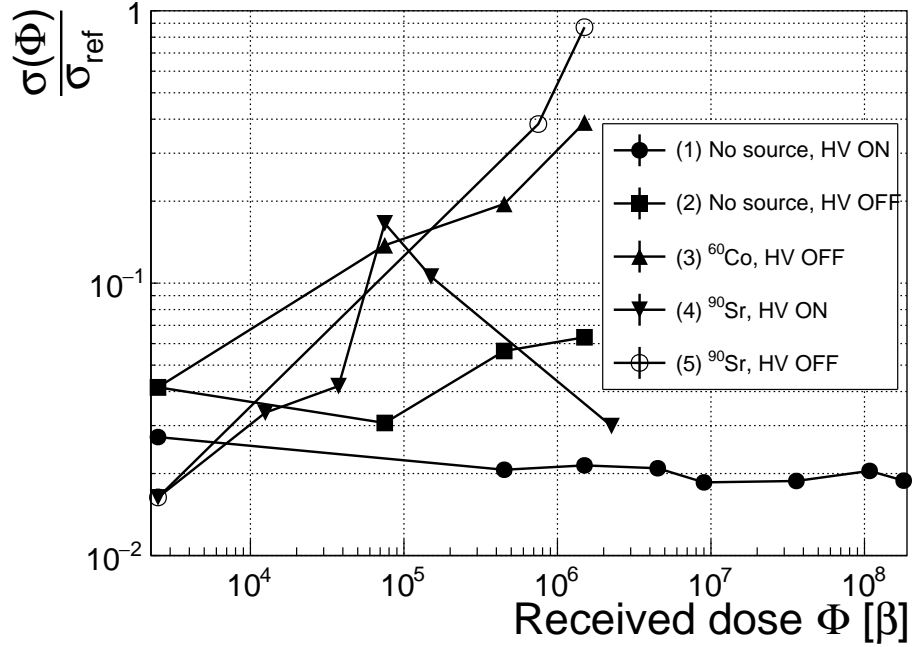


Figure 1.13: Comparison of the five procedures for the “healing” process for an irradiated diamond that had been exposed to α radiation with a rate of 10^1 s^{-1} , with the bias voltage switched on, for at least 30 minutes.

506 overall effect of the space-charge. The traps get filled with both flavours of carriers,
 507 thus they are neutralised. The pulse shape gradually returns to its initial state.

Procedure	Source	Type of radiation	Bias voltage	Effectiveness
1	/	/	ON	no
2	/	/	/	slow
3	^{60}Co	γ	/	YES
4	^{90}Sr	β	ON	no
5	^{90}Sr	β	/	YES

509 Table 1.2: Effectiveness of healing procedures.

510 In summary, the shape of the pulses caused by α radiation changes with time
 511 for irradiated samples. The shape of the pulses gets distorted and becomes erratic.
 512 Charge collection decreases and its spread increases. This happens even faster for
 513 non-primed diamonds. To “heal” the diamond – to bring the pulse shapes back to
 514 their initial shape – the sample must be primed using a β or a γ source for several
 515 minutes without bias voltage. Switching to the inverse polarity for a few seconds
 516 helps a bit, but in a long run distorts the signal, which cannot return to its initial
 517 shape.

518 **1.4 Temperature limitations**

519 A test has been carried out to evaluate the effect of temperature changes on the
520 output signal of the diamond sensors. A cryostat filled with liquid helium is used to
521 cool down the sensor during the measurement process. The current signal response
522 to α -particles is measured at 18 temperature points between 4 K and 295 K. At
523 every temperature point a set of 300 pulses is recorded at various bias voltages. The
524 resulting data show that the charge collection is stable from RT down to 150 K where
525 it starts decreasing. It stabilises again at about one third of the initial value at 75 K.
526 This behaviour was first measured and discussed by H. Jansen [13].

527 The band gap energy in diamond is equal to $E_g = 5.5$ eV while the average energy
528 to produce an electron-hole pair is $E_{e-h} = 13.25$ eV. This means there is excessive
529 energy deposited in the diamond bulk. The incident α -particle stops within $\sim 10\text{--}15$ μm of the bulk,
530 transferring all its energy to the lattice during deceleration. A part of this energy directly ionises the carbon atoms, creating free electron-hole pairs.

531 The remaining energy, however, is converted into lattice vibrations – phonons [20,
532 13]. In other words, the lattice within the ionisation volume (approximately $\sim 15 \mu\text{m} \times \sim 2 \text{ nm}$
533 in size) is briefly heated up. The hot plasma then cools down to the temperature of
534 the surrounding material by means of heat dissipation, i.e. phonon transport.

535 The free electron binds with the free hole into a bound state (not recombination)
536 – the exciton [16]. The exciton binding energy is 80 meV, which introduces an energy
537 level within the forbidden gap just under the conduction band. At higher temper-
538 atures the lattice provides enough energy to thermally excite the electron from the
539 exciton state back to the conduction band. At lower temperatures, however, the ex-
540 citon lifetime increases, which means that it takes a longer time for the electrons to
541 get re-excited to the conduction band. The re-excitation lifetime at room temper-
542 ature is ~ 30 ps, increasing to $\sim 150 \mu\text{s}$ at 50 K [13]. This means that some of the
543 bound electrons do not even start drifting within the period of ~ 10 ns, which is the
544 expected carrier drift time. When they are finally freed, the current they induce is
545 already hidden in the electronics noise. The effective area of the observed current
546 pulse is therefore smaller than that of a pulse induced by all the carriers drifting at
547 the same time. This in effect reduces the measured collected charge. The longer the
548 time constant, the lower the measured collected charge, as shown in section 1.4.2.

550 **1.4.1 Temperature-variant α -TCT before irradiation**

551 Three sCVD diamond samples have been tested at a range of temperatures using
552 the α -TCT technique. At each temperature point, the bias voltage is set to several
553 positive and negative values. A set of 300 pulses is recorded at every data point
554 and averaged offline. The resulting averaged pulses of sample S37 at the 260 K
555 temperature point and a bias voltage of ± 700 V, ± 500 V and ± 400 V are shown in
556 figure 1.14. The pulses induced by holes as charge carriers are shorter than those
557 induced by electrons, which means that holes travel faster in diamond. The area of

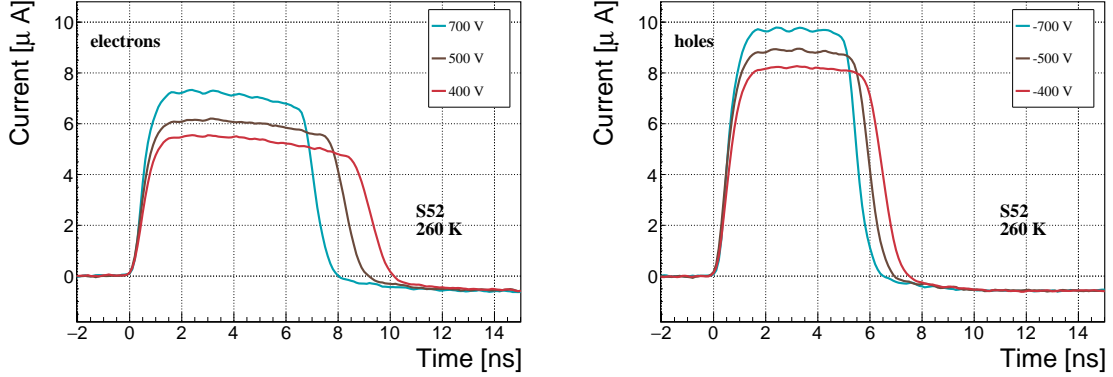


Figure 1.14: Varied bias voltage at a fixed temperature.

the pulse, however, is the same for both polarities, which corresponds to the fact that the same amount of charges is drifting in both cases.

Figure 1.15 shows pulses at a bias voltage set to ± 500 V across the range of temperatures between 4 K and 295 K. Several conclusions can be drawn by observing their shape. First, the pulse shapes change with decreasing temperature. The pulse time gets shorter and higher, hinting at the faster carrier drift velocity v_{drift} . Second, between 150 K and 75 K there is a significant change in shape - the time constant of the rising edge increases significantly and the pulse area decreases. From 75 K down to 4 K there is no significant change. Last, the top of the pulse at the S52 is not flat, which means that a portion of the drifting charge is lost along the way. This is due to charge trapping, likely by means of crystal defects or impurities.

1.4.2 Temperature-variant α -TCT after irradiation

The irradiated S79 and S52 have been re-tested in the cryostat after irradiation. The aim is to observe how their pulse shapes change with decreasing temperature, in particular the decaying top of the pulses, as shown in figure 1.16. The decay time gives information on trapping of charge carriers while travelling through the diamond bulk. A variation of the decay time constant as a function of temperature might help to reveal the type and depth of the charge traps. To observe these effects or lack thereof, a number of requirements have to be met. First, the diamond samples are intentionally not primed prior to the experiment because priming would improve the pulse shapes and possibly change the decay time constant of the signal. Second, keeping in mind that the pulse shape of irradiated diamonds changes with time, the duration of the measurement of an individual data point has to be short – of the order of 30 seconds. Last, the sequence of the bias voltage settings is important, the reason for which is explained below.

Unfortunately it is not possible to avoid temporal pulse changes. For instance, one measurement point takes approximately one minute. After the measurement, the bias voltage polarity is swapped for a few seconds to bring the diamond back into

1.4. TEMPERATURE LIMITATIONS

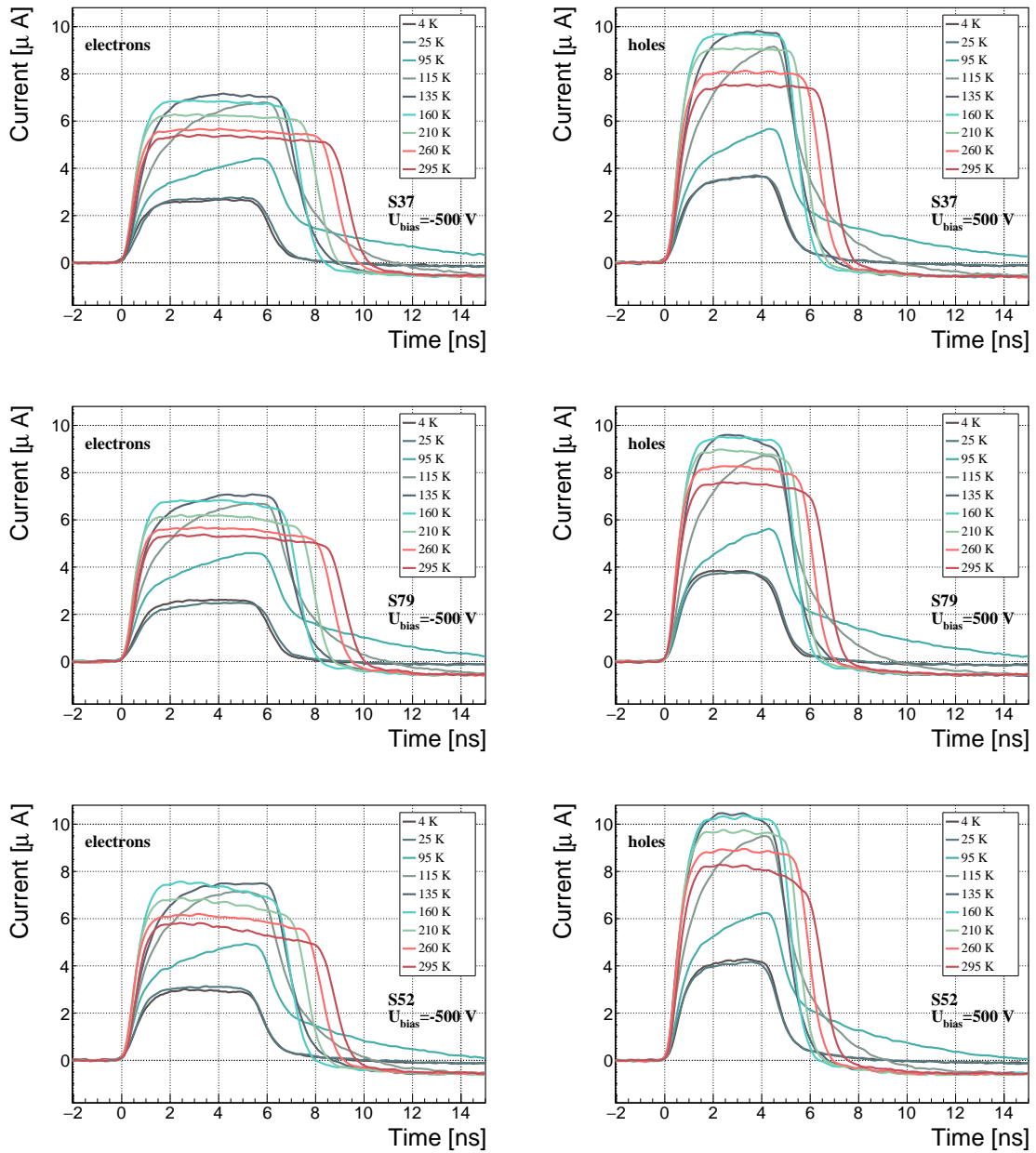


Figure 1.15: Several data points between 4 K and 295 K at a bias voltage of ± 500 V.

586 its initial state. But a few seconds with respect to a minute are not enough, but
587 due to time constraints this cannot be avoided. Therefore when the bias voltage is
588 set to the next value, there is still some residual effect of the previous measurement.
589 Similar to the effects of polarisation, this effect is also decreasing the pulse height.
590 This can be observed in figure 1.16, which shows the resulting pulses of S52 for bias
591 voltages of ± 200 V, ± 300 V, ± 400 V and ± 500 V at 230 K and 260 K. In this case
592 the measurement sequence is: 230K (200 V, 300 V, 400 V, 500 V, -500 V, -400 V,
593 -300 V), 260 K (-200 V, -300 V, -400 V, -500 V, 500 V, 400 V, 300 V). The changes in
594 pulse shapes for holes at 230 K and 260 K cannot be attributed to the temperature
595 change. Instead, the explanation could lie in diamond “polarisation”. This means
596 that, when exposed to an electric field with α measurements ongoing, an internal
597 electric field of inverse polarity builds up in the diamond, which effectively reduces
598 the overall electric field. This internal field does not dissipate when the external
599 bias voltage is switched off. The diamond becomes “polarised”. When switching the
600 polarity of the external bias voltage, the internal and external electric field point in
601 the same direction at the beginning, increasing the overall electric field and with it
602 the pulse height. In figure 1.16 this happens when switching from 500 V (figure 1.16a)
603 to -500 V (figure 1.16b) at 230 K. The built up polarisation contributes to the pulse
604 having a sharp rising edge and a high amplitude. This effect decays during the next
605 two voltage points. There would be a handful of ways to avoid this polarisation effect
606 in the data:

- 607 1. After every data point invert the bias voltage and leave it to return to a neutral
608 state for the same amount of time,
- 609 2. Make a hysteresis of data points, going from minimum negative to maximum
610 positive bias several times,
- 611 3. Reduce the measurement time at every bias voltage setting.

612 Unfortunately, options (1) and (2) are very time consuming and would increase the
613 overall experiment time to over one day. The third option would worsen the resulting
614 averaged pulses. In the end an alternative option has been chosen: alternating the
615 starting bias voltage and the sequence at every temperature point. With this option,
616 a meaningful systematic error in analysing the pulse shapes can be attained.

617 Figure 1.17 shows the irradiated S52 and S79 as well as the non-irradiated S37
618 for comparison, all at a bias voltage of ± 500 V and at several temperature points
619 between 4 K and 295 K. It is evident that the radiation damage affects the shape of
620 the pulses across all temperatures.

621 **Collected charge as a function of temperature**

622 The area below the current pulse is proportional to the charge collected by the dia-
623 mond detector. The collected charge is measured as a function of temperature. First,
624 the amplitude values of the averaged pulses at a bias voltage of ± 500 V and across

1.4. TEMPERATURE LIMITATIONS

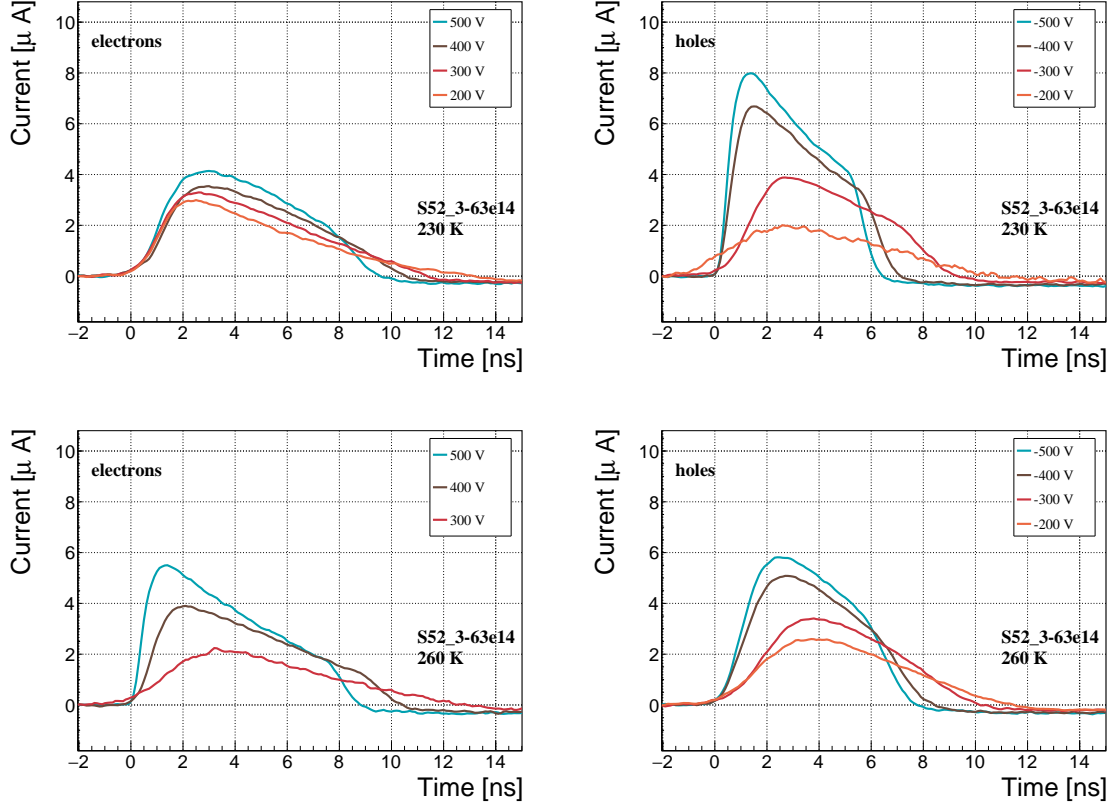


Figure 1.16: Varied bias voltage at a fixed temperature for an irradiated sample.

the temperature range between 4 K and 295 K have to be integrated. Then a calibration factor is used to derive the charge for all data points. This factor is obtained using a Cx charge-sensitive amplifier. The resulting values for electrons and holes are plotted in figures 1.18 and 1.19, respectively. The drop in collected charge and a first model is given in [13]. In the framework of this thesis the focus is on the effect in the irradiated devices. The new contribution are the data points for the irradiated samples. The values for all samples are fairly stable in the range between 4 K and 75 K and between 150 K and 295 K. However, in the values for the irradiated S52 some excursions can be observed. This is due to the sequence of the measurement steps, which results in a hysteresis effect explained in the preceding text.

The collected charge drops significantly from 150 K down to 75 K. In the non-irradiated samples the values in the lower temperature range are approximately 30 % of the values in the high range. For the irradiated samples this difference is lower – 35 % for S79 and 50 % for S52.

An interesting detail in figure 1.18 is that the ratio between the values for non-irradiated samples and their irradiated counterparts at the lower temperature range is different than at the higher range. In other words, the charge loss due to irradiation damage is lower for temperatures between 4 K and 75 K than for temperatures between 150 K and 295 K. The irradiated S52 collects 78 % of the initial charge in the low

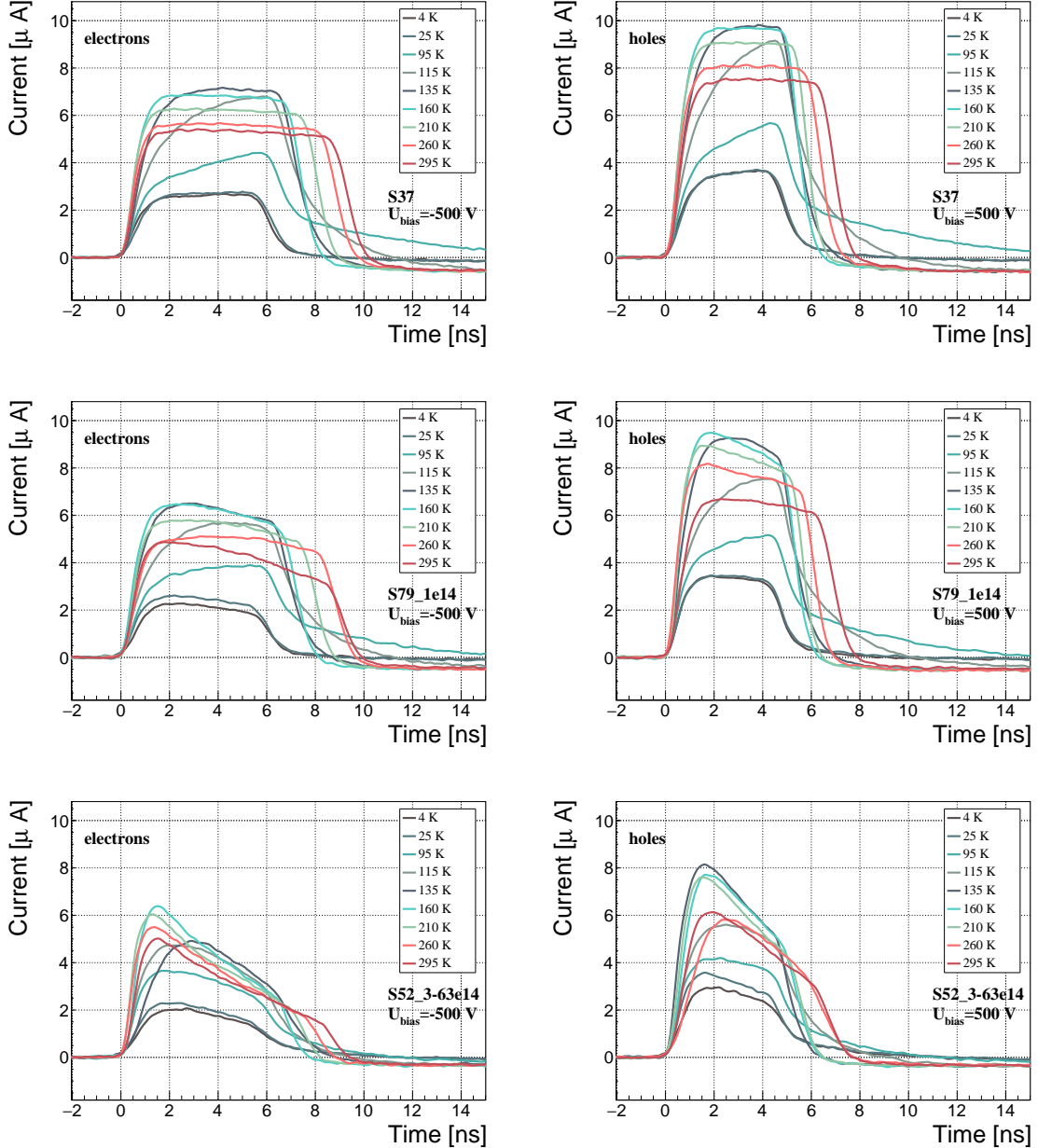


Figure 1.17: After irradiation: several data points between 4 K and 295 K at a bias voltage of ± 500 V.

temperature range, but only 59 % of the initial charge for the high range. The values for S79 for these two temperature ranges are 100 % and 90 %, which means that the drop in charge collection efficiency after irradiation to $1 \times 10^{14} \pi \text{ cm}^{-2}$ is negligible for temperatures below 75 K.

1.4. TEMPERATURE LIMITATIONS

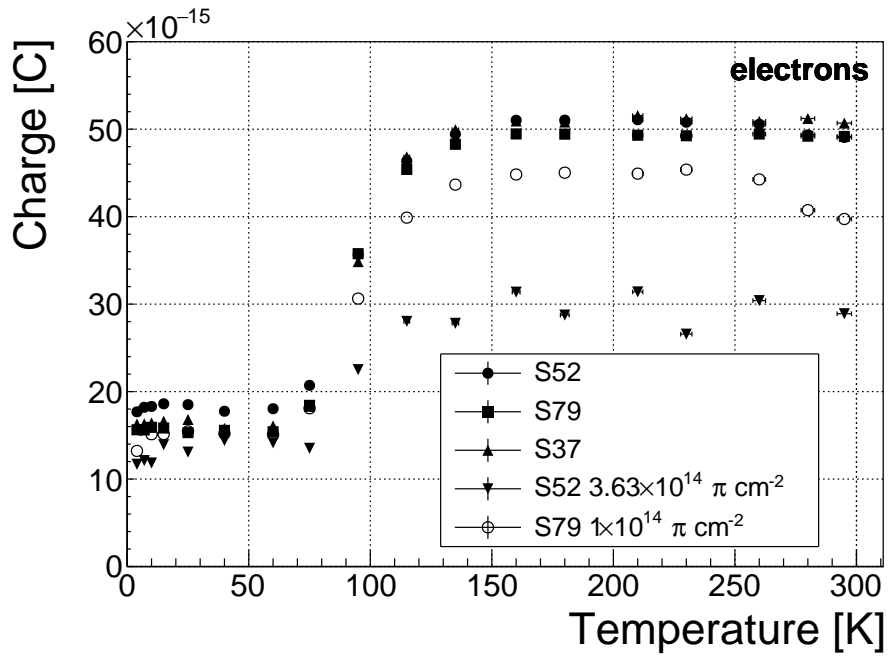


Figure 1.18: Collected charge for electrons as a function of temperature.

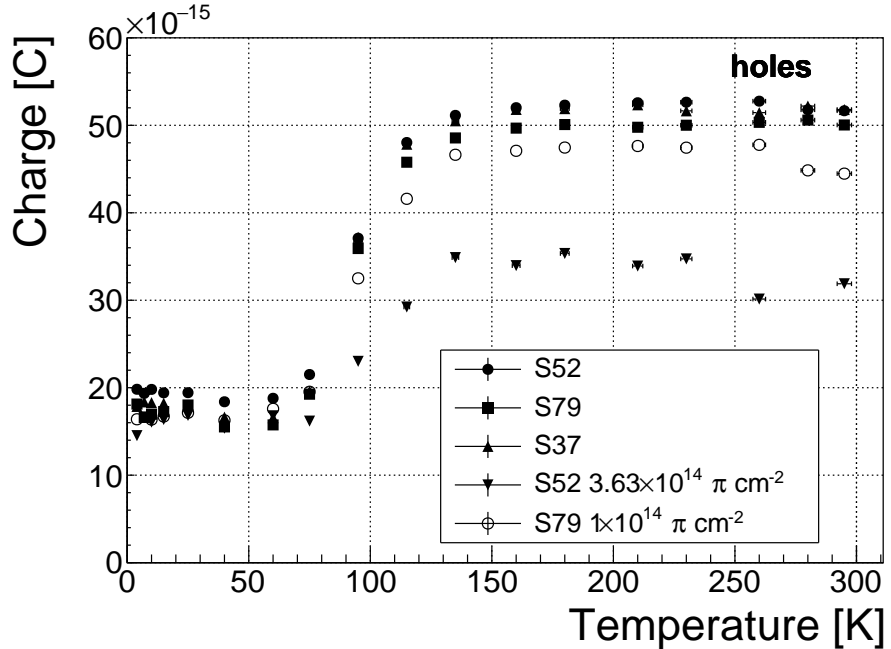


Figure 1.19: Collected charge for holes as a function of temperature.

648 Charge trapping

649 The charge carriers that drift through the bulk get stopped in the charge traps with
 650 a certain probability. This trapping happens uniformly throughout the diamond. In
 651 other words, the number of carriers in the moving charge cloud is gradually reduced.

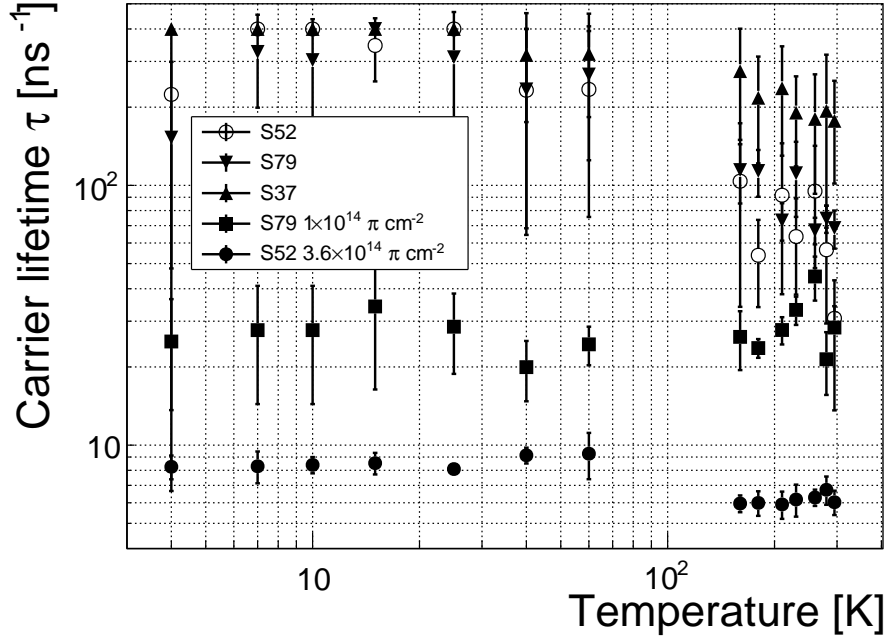


Figure 1.20: This figure shows the charge carrier lifetime as a function of temperature. The data points between 75 K and 150 K are omitted. The fit function only works well on signals with a well pronounced decaying top.

652 This in turn reduces the induced current. The function for the number of drifting
653 carriers per unit of length is a decaying exponential function:

$$I(t) = I_0 + I(0) \cdot e^{-\frac{t-t_0}{\tau}}, \quad (1.13)$$

654 where $I(0)$ is the initial induced current, I_0 is the end current, t is time, t_0 is temporal
655 displacement of the pulse and τ is the decay time constant. This value describes how
656 long it takes before the amplitude of the pulse decreases to 63 % of its initial height.

657 The decaying exponential function is fitted to the decaying top of the averaged
658 pulses at a bias voltages of ± 400 V and ± 500 V across all temperatures excluding
659 the transitional range between 75 K and 150 K. The resulting decay time constants
660 τ for an individual temperature point are not equal, which stems from the fact that
661 the pulses change with time due to “polarisation”. This counts as a systematic error.
662 Therefore the fitted τ for ± 400 V and ± 500 V are averaged into one value representing
663 the measurement at that temperature point. Figure 1.20 shows the fitted τ for the
664 five samples between 4 K and 295 K. In principle the time constants should be infinite
665 for a perfect and non-irradiated sample. Here a slightly tilted top of the pulse due to
666 space-charge is already successfully fitted with an exponential function (a pitfall in an
667 automatic analysis), resulting in a τ of the order of $(200 \pm 20) \times 10^{-9}$ s. Consequently
668 the fitting method is not adequate for non-irradiated samples. For the irradiated
669 samples the fit becomes increasingly more meaningful. As seen in figure 1.20, the
670 fitted values of the irradiated samples are fairly stable across all temperatures. There

1.4. TEMPERATURE LIMITATIONS

is a slight increase in the decay time constant of the S52 from $(6.0 \pm 0.5) \times 10^{-9}$ s above 150 K to $(8.5 \pm 0.9) \times 10^{-9}$ s below 75 K. On the other hand, this step is not observable in the S79 data. With only one sample exhibiting this behaviour, the effect is not significant enough. Judging by the data acquired, the samples would need to be irradiated to doses above $1 \times 10^{14} \pi \text{ cm}^{-2}$ to quantify this effect in detail. So far this effect is not regarded as significant for the scope of this thesis. Building on this assumption, the conclusion is that the signal decay time constant for irradiated sCVD diamond is constant across the temperature range between 4 K and 295 K, excluding the transitional range between 75 K and 150 K where it cannot be quantified properly.

Taking into account the discussion above, all the values can be averaged into one decay constant. Figure 1.21 shows these values for all samples as a function of the received $\pi_{300 \text{ MeV}}$ radiation dose. To estimate the charge carrier lifetime with respect to the radiation dose received, a similar model is used than that in section 1.5. This model states that the charge carrier lifetime is linearly decreasing with increasing radiation dose:

$$\frac{1}{\tau} = \frac{1}{\tau_0} + \kappa_\tau \cdot \Phi \quad (1.14)$$

$$\tau = \frac{\tau_0}{\kappa_\tau \tau_0 \Phi + 1} \quad (1.15)$$

where τ_0 is the lifetime for a non-irradiated sample (real lifetime, therefore of the order of 400 ns), τ is the lifetime of an irradiated sample, Φ is the received radiation dose and κ_τ the lifetime degradation factor. For these data the fitted factor is equal to $\kappa_\tau = (3.5 \pm 0.8) \times 10^{-16} \text{ s cm}^2 \pi_{300 \text{ MeV}}^{-1}$. Using this factor, the steepness of the decay in the pulse shape as a function radiation dose can be estimated. This is highly useful information when designing a system where the current pulse shape is an important factor.

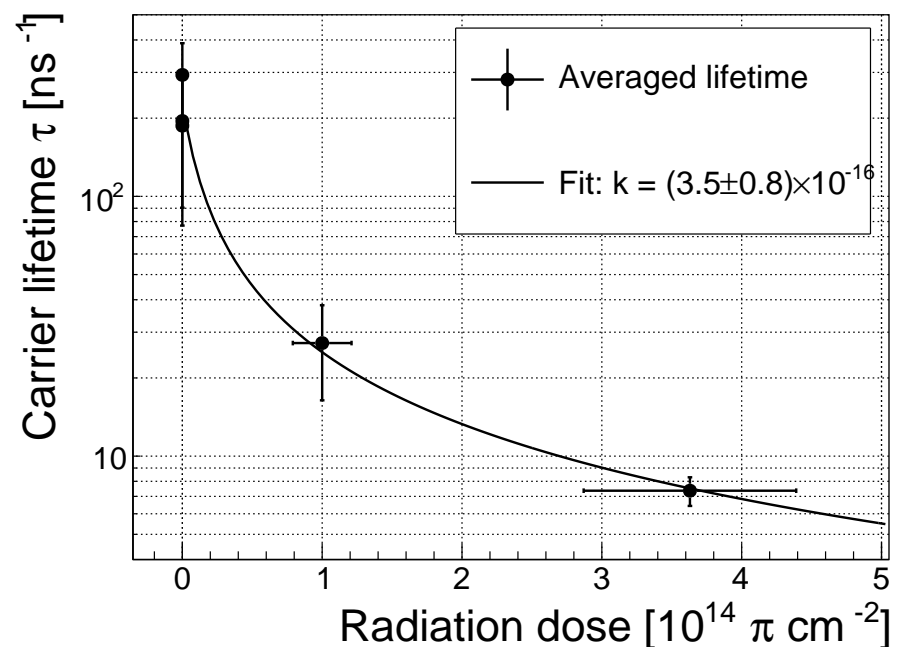


Figure 1.21: This figure shows the carrier lifetime averaged over all temperatures and plotted as a function of the π irradiation dose.

694 1.5 Conclusion

695 This chapter gives an overview of the capabilities and limitations of diamond as a
696 particle detector. Two effects on diamond are studied – radiation and temperature.

697 Two sCVD diamond detectors were irradiated with 300 MeV pions. They were
698 tested alongside a non-irradiated sample to observe the changes in the ability to detect
699 α , β and γ radiation. Their charge collection efficiency was measured in a test beam
700 facility. The results were compared to the results from the RD42 collaboration and
701 a DPA model. A radiation damage factor $k_\lambda = (4.4 \pm 1.2) \times 10^{-18} \mu\text{m}^{-1} \text{cm}^{-2}$ was
702 obtained for $\pi_{300 \text{ MeV}}$ particles. The data point was not in agreement with the data
703 provided by RD42 nor with the model. However, the irradiation process and the low
704 number of tested samples hold a relatively high statistical uncertainty. In addition,
705 there was no diamond surface treatment done in between the measurements, as is
706 the case in the study conducted by RD42. The results obtained in the course of
707 these measurements are going to be fed into the existing pool of data in the RD42
708 collaboration.

709 The next step was to test the long-term capabilities for α detection. The shape
710 of the ionisation profile was investigated to determine the behaviour of the charge
711 carriers in the irradiated diamond. An exponential decay was observed in the pulses
712 of irradiated samples, proving that there are charge traps in the bulk that were created
713 during irradiation. Then a long-term stability test was carried out. The results show
714 that the irradiated diamond detectors do not provide a stable and reliable long-term
715 measurement of α particles. This might be due to a space-charge build-up in the
716 bulk, which changes the electric field, affecting the charge carriers. A procedure to
717 improve the pulse shape using β and γ radiation was proposed.

718 Finally, the diamond sensors were cooled down to temperatures between 4 K and
719 295 K. Their response to α particles was observed. The results of the non-irradiated
720 and irradiated samples were compared. The effect of reduction for the number of
721 drifting charges due to exciton recombination was observed in both sets of data.
722 The second set had a superimposed effect of charge trapping during the drift, which
723 was represented by an exponential decay in the signal. The decay time constant
724 did not change with temperature. Therefore all temperature points for individual
725 samples were averaged and the decay time constants were plotted against the received
726 radiation dose. A lifetime degradation factor $\kappa_\tau = (3.5 \pm 0.8) \times 10^{-16} \text{ s cm}^2 \pi_{300 \text{ MeV}}^{-1}$
727 for non-primed diamonds was defined.

⁷²⁸ Bibliography

- ⁷²⁹ [1] *DRS4*. <https://www.psi.ch/drs/evaluation-board>.
- ⁷³⁰ [2] *Element Six*. <http://www.e6.com>.
- ⁷³¹ [3] *IIa Technologies Pte. Ltd.* <https://www.2atechnologies.com>.
- ⁷³² [4] *Paul Scherrer Institute*. <https://www.psi.ch/>.
- ⁷³³ [5] *RD42 collaboration*. <http://rd42.web.cern.ch/rd42/>.
- ⁷³⁴ [6] *Determination of operational dose equivalent quantities for neutrons*. ICRU,
⁷³⁵ Washington, DC, 2001.
- ⁷³⁶ [7] H. Bethe and J. Ashkin. *Experimental Nuclear Physics*, ed. E. Segre, page 253,
⁷³⁷ 1953.
- ⁷³⁸ [8] Giorgio Brianti. SPS North Experimental Area. Technical Report CERN-SPSC-
⁷³⁹ T-73-8. LabII-EA-Note-73-4, CERN, Geneva, 1973.
- ⁷⁴⁰ [9] P. Carazzetti and H. R. Shea. *Electrical breakdown at low pressure for planar
741 microelectromechanical systems with 10- to 500 μm gaps*. *J. Micro/Nanolith.
742 MEMS MOEMS*, (8(3), 031305), Jul-Sep 2009.
- ⁷⁴³ [10] E. Griesmayer and B. Dehning. Diamonds for beam instrumentation. *Physics
744 Procedia*, 37:1997 – 2004, 2012. Proceedings of the 2nd International Conference
745 on Technology and Instrumentation in Particle Physics (TIPP 2011).
- ⁷⁴⁶ [11] Moritz Guthoff, Wim de Boer, and Steffen Mller. Simulation of beam induced
747 lattice defects of diamond detectors using {FLUKA}. *Nuclear Instruments and
748 Methods in Physics Research Section A: Accelerators, Spectrometers, Detectors
749 and Associated Equipment*, 735:223 – 228, 2014.
- ⁷⁵⁰ [12] M. Huhtinen. Simulation of non-ionising energy loss and defect formation in
751 silicon. *Nuclear Instruments and Methods in Physics Research A*, 491:194–215,
752 September 2002.
- ⁷⁵³ [13] Hendrik Jansen, Norbert Wermes, and Heinz Pernegger. *Chemical Vapour De-
754 position Diamond - Charge Carrier Movement at Low Temperatures and Use in*

BIBLIOGRAPHY

- 755 *Time-Critical Applications*. PhD thesis, Bonn U., Sep 2013. Presented 10 Dec
756 2013.
- 757 [14] Claude A. Klein. Radiation-induced energy levels in silicon. *Journal of Applied
758 Physics*, 30(8):1222–1231, 1959.
- 759 [15] Gregor Kramberger, V. Cindro, A. Gorisek, I. Mandic, M. Mikuz, and M. Zavr-
760 tanik. Effects of bias voltage during priming on operation of diamond detectors.
761 *PoS*, Vertex2012:013, 2013.
- 762 [16] W. Y. Liang. Excitons. *Physics Education*, 5:226–228, July 1970.
- 763 [17] M. Mikuž. *Diamond sensors for high energy radiation and particle detection*.
764 TIPP, 2011.
- 765 [18] V. Sarin. *Comprehensive Hard Materials*. Elsevier Science, 2014. p. 411.
- 766 [19] M. Červ, P. Sarin, H. Pernegger, P. Vageeswaran, and E. Griesmayer. Diamond
767 detector for beam profile monitoring in comet experiment at j-parc. *Journal of
768 Instrumentation*, 10(06):C06016, 2015.
- 769 [20] J. L. Yarnell, J. L. Warren, and R. G. Wenzel. Lattice vibrations in diamond.
770 *Phys. Rev. Lett.*, 13:13–15, Jul 1964.